Fractalkine-induced microglial vasoregulation occurs within the retina and is altered early in diabetic retinopathy

Samuel A. Mills[a,1], Andrew I. Jobling[a,1], Michael A. Dixon[a,1], Bang V. Bui[b], Kirstan A. Vessey[a], Joanna A. Phipps[a], Ursula Greferath[a], Gene Venables[a], Vickie H. Y. Wong[b], Connie H. Y. Wong[c], Zheng He[b], Flora Hui[b,d], James C. Young[a], Josh Tonc[a], Elena Ivanova[e], Botir T. Sagdullaev[e], and Erica L. Fletcher[a,2]

[a]Department of Anatomy and Physiology, University of Melbourne, Parkville, 3010 VIC, Australia; [b]Department of Optometry and Vision Sciences, University of Melbourne, Parkville, 3010 VIC, Australia; [c]Department of Medicine, Centre for Inflammatory Diseases, School of Clinical Sciences, Monash University, Clayton, 3800 VIC, Australia; [d]Centre for Eye Research Australia, Royal Victorian Eye and Ear Hospital, East Melbourne, 3002 VIC, Australia; and [e]Burke Neurological Institute, Weill Cornell Medical College, White Plains, NY 10605

Edited by Jeremy Nathans, Molecular Biology and Genetics, The Johns Hopkins University School of Medicine, Baltimore, MD; received July 8, 2021; accepted October 14, 2021

Local blood flow control within the central nervous system (CNS) is critical to proper function and is dependent on coordination between neurons, glia, and blood vessels. Macroglia, such as astrocytes and Müller cells, contribute to this neurovascular unit within the brain and retina, respectively. This study explored the role of microglia, the innate immune cell of the CNS, in retinal vasoregulation, and highlights changes during early diabetes. Structurally, microglia were found to contact retinal capillaries and neuronal synapses. In the brain and retinal explants, the addition of fractalkine, the sole ligand for monocyte receptor Cx3cr1, resulted in capillary constriction at regions of microglial contact. This vascular regulation was dependent on microglial Cx3cr1 involvement, since genetic and pharmacological inhibition of Cx3cr1 abolished fractalkine-induced constriction. Analysis of the microglial transcriptome identified several vasoactive genes, including angiotensinogen, a constituent of the renin-angiotensin system (RAS). Subsequent functional analysis showed that RAS blockade via candesartan abolished microglial-induced capillary constriction. Microglial regulation was explored in a rat streptozotocin (STZ) model of diabetic retinopathy. Retinal blood flow was reduced after 4 wk due to reduced capillary diameter and this was coincident with increased microglial association. Functional assessment showed loss of microglial–capillary response in STZ-treated animals and transcriptome analysis showed evidence of RAS pathway dysregulation in microglia. While candesartan treatment reversed capillary constriction in STZ-treated animals, blood flow remained decreased likely due to dilation of larger vessels. This work shows microglia actively participate in the neurovascular unit, with aberrant microglial–vascular function possibly contributing to the early vascular compromise during diabetic retinopathy.

retina | microglia | capillary regulation | fractalkine | diabetes

The retina is one of the most metabolically active organs in the body, and in most mammals is supplied by outer (choroidal) and inner (retinal) vascular networks (1). While the choroid provides for the light-detecting photoreceptors within the outer retina, the retinal blood supply supports the numerous neurons and glia found in the ganglion cell and inner nuclear layers (2). The arterioles of the retinal blood supply enter at the optic disk and branch to form sequentially smaller vessels, including retinal capillaries, establishing the superficial vascular plexus. These capillaries penetrate the inner retina, forming the relatively sparse intermediate vascular plexus, and deeper toward the outer retina forming the highly anastomosed deep vascular plexus. Completing the vascular circuit, blood returns via the venules on the retinal surface, which exit alongside the optic nerve (3, 4).

Blood flow throughout the retina is largely dependent on vessel caliber, which is tightly regulated to meet the metabolic demands of neuronal activity (5). An example of this is the well-defined hyperemic response, whereby increased neuronal activity (via flickering light) results in arteriole dilation and increased inner retinal blood flow (6). Unlike peripheral blood vessels, retinal and brain vasculature have no direct neuronal input to modulate vascular tone; rather, macroglial cells (Müller cells and astrocytes) are thought to actively regulate vascular caliber in response to changes in neural activity (7, 8). This type of coupling has given rise to the idea of a neurovascular unit, encompassing neurons, glia, and blood vessels (7). While studies within the retina identified neuronal-dependent calcium increase in Müller cells to mediate vessel diameter change (9), more recent data

Significance

This work identifies a role for microglia, the innate immune cells of the CNS, in the local control of the retinal vasculature and identifies deficits early in diabetes. Microglia contact neurons and vasculature and express several vasoactive agents. Activation of microglial fractalkine-Cx3cr1 signaling leads to capillary constriction and blocking the renin-angiotensin system (RAS) with candesartan abolishes microglial-mediated vasoconstriction in the retina. In early diabetes, reduced retinal blood flow is coincident with capillary constriction, increased microglial–vessel association, loss of microglial–capillary regulation, and altered microglial expression of the RAS pathway. While candesartan restores retinal capillary diameter early in diabetes, targeting of microglial–vascular regulation is required to prevent coincident dilation of large retinal vessels and reduced retinal blood flow.

Author contributions: S.A.M., A.I.J., M.A.D., B.V.B., and E.L.F. designed research; S.A.M., A.I.J., M.A.D., B.V.B., K.A.V., J.A.P., U.G., G.V., V.H.Y.W., C.H.Y.W., Z.H., F.H., J.C.Y., J.T., E.I., and B.T.S. performed research; S.A.M., A.I.J., M.A.D., K.A.V., U.G., G.V., V.H.Y.W., C.H.Y.W., Z.H., F.H., J.C.Y., J.T., E.I., B.T.S., and E.L.F. analyzed data; and S.A.M., A.I.J., B.V.B., and E.L.F. wrote the paper.

The authors declare no competing interest.

This article is a PNAS Direct Submission.

[1]S.A.M., A.I.J., and M.A.D. contributed equally to this work.

[2]To whom correspondence may be addressed. Email: e.fletcher@unimelb.edu.au.

This article contains supporting information online at http://www.pnas.org/lookup/suppl/doi:10.1073/pnas.2112561118/-/DCSupplemental.

Published December 13, 2021.

suggest regulation of the inner retinal vasculature is more complex (10). Evidence for this comes from the fact that the same light stimulus can induce either vasoconstriction or vasodilation, and Müller cell-dependent calcium signaling only controls capillaries within the intermediate vascular plexus (11, 12). This suggests the existence of multiple regulatory pathways within the retina.

Recently, it has been proposed that microglia, the innate immune cells of the retina, may also play a role in the neurovascular unit, although direct functional evidence is lacking (13). The conventional view of microglia is that they contribute to disease via the release of proinflammatory and neurotoxic cytokines (14–16). However, it is now recognized that microglia play several important, inflammation-independent roles in the normal brain and retina, such as dynamic synaptic surveillance and synaptic pruning (17–19). Within the retina, microglia are known to be in close contact with the vasculature and impact on vessel development (20). Despite this, the inflammation-independent response of microglia to neuronal signaling and their role in the regulation of vascular tone has yet to be confirmed.

While regulation of retinal blood flow is critical to function (21), vascular dysfunction is known to occur in several pathologies, including diabetic retinopathy (DR). Early in the progression of DR, vascular pathology such as reduced retinal blood flow, microaneurysms, and areas of vascular nonperfusion occur (22). Reduced retinal blood flow, in particular, presents early in humans with diabetes (23–25) and in animal models of diabetes (25). Altered inner retinal vascular regulation is considered a likely precursor to the development of severe vascular pathology in DR (26).

The present study investigates whether retinal microglia form a functional component of the neurovascular unit, and whether signaling through the fractalkine-Cx3cr1 pathway modulates vascular diameter. In addition, the work explores whether altered microglial involvement with the inner retinal vasculature may help explain the reduced retinal blood flow that occurs early during diabetes. Exploring the mechanisms responsible for the tight regulation between neuronal activity and the local blood supply is critical to understanding retinal function in health and disease and may provide an empirical framework for future therapies targeting vascular pathogenesis.

Results

Microglia Contact both Retinal Vasculature and Neuronal Synapses. Microglia within the central nervous system (CNS) have a close association with the vasculature, particularly during development, injury, and disease (20, 27). However, less is known about microglial–vascular interactions in normal tissue. Within the retina, microglial cell bodies typically reside in the plexiform layers, while their processes extend throughout the retina (*SI Appendix*, Fig. S1). Inspection of the superficial vascular plexus shows microglia tiling the whole tissue (Fig. 1*A*, enhanced green fluorescent protein [EGFP], green) and in close association with retinal vasculature (Fig. 1 *A*, *Inset*; isolectin B4 [IB4], red). When microglial process contact with retinal vessels of different diameters is quantified relative to the respective area of each vessel diameter class, microglia are seen to interact with smaller retinal vessels (≤15 μm), particularly the smallest retinal capillaries (<10 μm), when compared to the larger vessels (Fig. 1*B*) (one-way ANOVA, $P < 0.05$, 0.001 for 15 to 20 μm and >20 μm, respectively). At the ultrastructural level (Fig. 1*C*), a microglial process (stained for EGFP) abuts a pericyte, which lies over an endothelial cell lining the capillary lumen. This microglial–pericyte contact is also investigated immunohistochemically using the NG2-DsRed reporter mouse, which labels pericyte somata and processes (Fig. 1*D*, red). A microglial cell (Fig. 1*D*, Iba-1, green) is observed to contact two pericyte somata (Fig. 1*D*, red), with nuclei immunolabeled with DAPI (Fig. 1*D*, blue). Orthogonal projections (Fig. 1*D*, top and right) from the boxed area, show direct contact between the two cell types. The contact (Fig. 1*D*, asterisk) was further imaged at higher resolution to show direct contact between the microglial process (Fig. 1*D*, green) and pericyte soma (red; asterisk in Fig. 1*E*; also see *SI Appendix*, Fig. S2 and Movie S1). The extent of microglial contact with pericyte somata, processes (NG2-labeled) and capillary areas devoid of pericyte contact ($NG2^-/IB4^+$ regions, likely endothelial cells) was quantified in rat retina, with no preference observed for microglial–pericyte or microglial–vessel contact (Fig. 1*F*).

In addition to contacting retinal vessels (IB4, magenta, asterisk in Fig. 1*G*), microglia (EGFP, green) are also observed to extend processes into the inner plexiform layer, where neuronal synapses reside (Fig. 1*G*, VGLUT1 red, arrowheads; DAPI blue). The Fig. 1 *G*, *Inset* shows a rendering of microglial–neuronal interactions at higher magnification. This is also observed in the human retina (Fig. 1*H*, DAPI, blue) with microglia (Iba-1, green) contacting both retinal vessels (Fig. 1*H*, vitronectin, magenta, asterisk) and neuronal synapses (Fig. 1*H*, VGLUT1, red. arrowheads). When quantified in the $Cx3cr1^{+/GFP}$ mouse retinae, the majority of microglia (Fig. 1*I*, EGFP, green) in the inner retina contact both neuronal synapses (Fig. 1*I*, VGLUT1, blue) and retinal vessels (IB4, red; Fig. 1 *I*, *Inset*) (73 ± 13%, rat retina). Individual channels for immunolocalization are shown in *SI Appendix*, Fig. S3.

Microglia Modulate Vessel Diameter and Express Vasoactive Genes. Within the brain and retina, macroglial (astrocyte and Müller cell) cell contact with neuronal synapses and vasculature is critical for local control of blood supply in response to neuronal activity (7, 8). To determine whether microglia play a similar role, $Cx3cr1^{GFP/+}$ retinae were isolated and maintained ex vivo. Microglia were visualized via their expression of EGFP (Fig. 2*A*, green) and vessels were labeled with rhodamine B (Fig. 2*A*, red). As the fractalkine-Cx3cr1 axis is thought to mediate neuronal–microglial communication, blood vessels and microglia were imaged while fractalkine (200 ng/mL) or PBS was perfused into the chamber (Movie S2). Vessel diameter change was monitored and expressed relative to the baseline value for the same region of vessel.

In response to fractalkine, blood vessel regions that were associated with microglial processes (m+) constricted (Fig. 2*B*, m+) (two-way ANOVA; PBS vs. fractalkine, $P < 0.001$), while those regions that were further away from microglial processes (m−) exhibited no significant alteration in capillary diameter (Fig. 2*B*, m−) (two-way ANOVA; PBS vs. fractalkine, $P = 0.26$). These ex vivo preparations showed minimal microglial process movement at the vascular level throughout the imaging, including during fractalkine exposure (*SI Appendix*, Fig. S4 and Movie S2). When explants lacking Cx3cr1 ($Cx3cr1^{GFP/GFP}$ mouse) were exposed to fractalkine, no alteration in vessel diameter was observed compared to PBS controls at regions with (m+; 105.7± 2.7% vs. 94.7 ± 2.3%, two-way ANOVA $P = 0.52$) or without (m−; 98.8 ± 1.2% vs. 97 ± 1.3%, two-way ANOVA $P = 0.999$) microglial contact (Fig. 2*B*). Further supporting a Cx3cr1-dependent mechanism, preincubation with the Cx3cr1 inhibitor, AZD8797 (28), inhibited fractalkine (FKN)-induced constriction (Fig. 2 *B*, *Inset*) (FKN 82 ± 2%, FKN+AZD8797 96 ± 2%, *t* test $P = 0.015$). Finally, to explore whether this vasomodulatory function of fractalkine was retina-specific, superficial vessels within the rat brain were imaged using a thin skull preparation. These preliminary data showed that while vehicle delivery resulted in no alteration in vessel diameter, the subdural addition of fractalkine lead to a significant constriction of the smaller vessels (Fig. 2*C*) (repeated-measures two-way

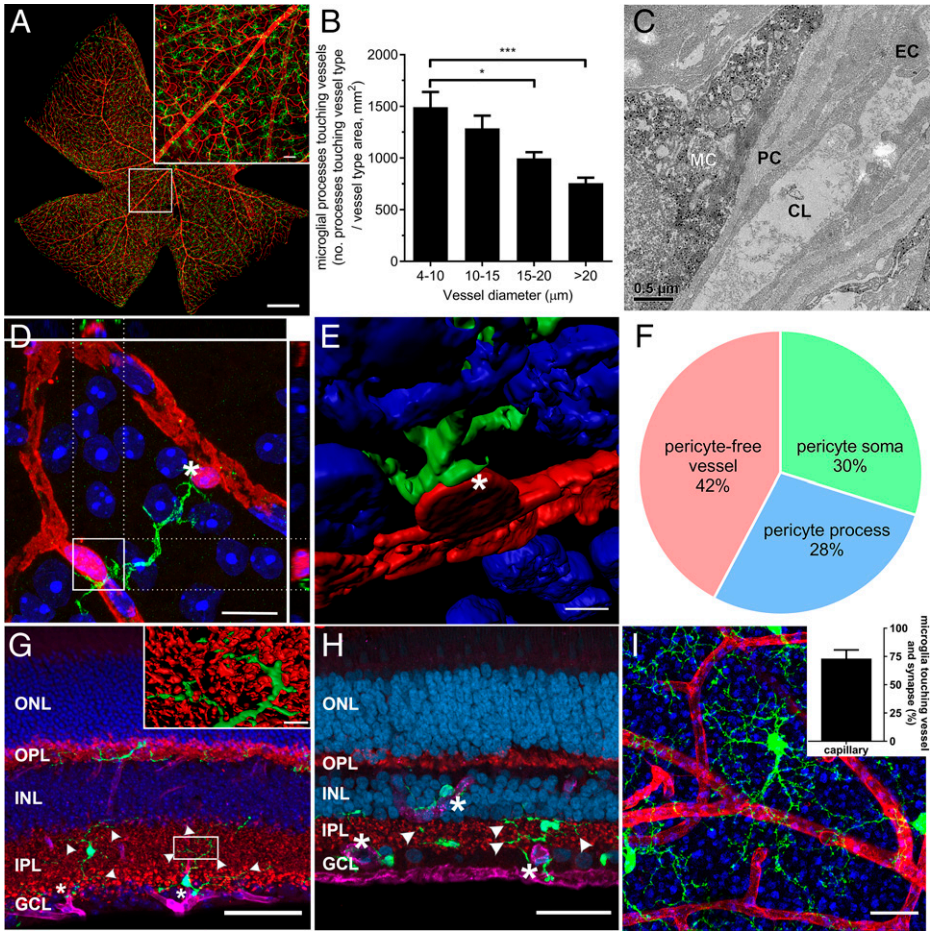

Fig. 1. Retinal microglia associate with vasculature and neuronal synapses. (*A*) Whole-mounted mouse retina (*Cx3cr1*$^{GFP/+}$) was labeled with anti-EGFP (microglia, green), and *G. simplicifolia* IB4 (blood vessels, red). The highlighted region shows microglial association with vessels within the superficial vascular plexus (*Inset*). (Scale bars, 500 μm; 50 μm, *Inset*.) (*B*) The association of microglial processes with vessels of different diameters within the superficial plexus was quantified relative to vessel area for each vessel size and show microglia preferentially associate with capillaries, **P* < 0.05, ****P* < 0.001. (*C*) The ultrastructure of microglia–vessel contact within the *Cx3cr1*$^{GFP/+}$ retina shows microglial processes (immunolabeled against EGFP, black dots) adjoin pericytes, which contact the endothelial cells lining the capillary lumen. (Scale bar, 0.5 μm.) (*D*) A whole-mounted retina from the NG2-DsRed pericyte reporter mouse (pericyte somata, processes, red) stained with Iba-1 (microglia, green) and DAPI (nuclei, blue) shows a microglial process making contact with pericyte somata. The boxed region is shown in orthogonal projections (above and right). (Scale bar, 10 μm.) (*E*) A high-resolution–rendered image of microglial–pericyte contact taken from asterisk in *D*. (Scale bar, 5 μm.) (*F*) Microglial–pericyte interaction was further probed in rat retina and the extent of contact with pericyte somata, processes (NG2$^-$) and capillary areas lacking pericyte contact (NG2$^-$/IB4$^+$) quantified. (*G*) A vertical section from a *Cx3cr1*$^{GFP/+}$ retina labeled for blood vessels (IB4, magenta), microglia (EGFP, green), neuronal synapses (VGLUT1, red), and cell nuclei (DAPI, blue), showing microglia contact retinal vessels (asterisk) and neuronal synapses (arrowheads). The boxed region was imaged at higher resolution and rendered to highlight microglial–synapse interaction (*Inset*). (Scale bars, 50 μm; 5 μm, *Inset*.) (*H*) Neuronal–microglial–vascular contact is also observed in human retina (microglia, Iba-1, green; vessels, vitronectin, magenta, asterisk; neuronal synapses, VGLUT1, red, arrowheads; cell nuclei, DAPI, blue). (Scale bar, 50 μm.) (*I*) When neuronal–microglial contact was quantified in the *Cx3cr1*$^{+/GFP}$ mouse at the level of the inner retina (vessels, IB4, red; microglia, EGFP, green; neuronal synapses VGLUT1, blue), the majority of microglia contact both neuronal synapses and vessels. (Scale bar, 20 μm.) Data presented as mean ± SEM, $n = 5$ (*B* and *F*), $n = 3$ (*I*, *Inset*). GCL, ganglion cell layer; INL, inner nuclear layer; IPL, inner plexiform layer; MC, microglia; PC, pericyte; EC, endothelial cell; CL, capillary lumen; ONL, outer nuclear layer; OPL, outer plexiform layer.

ANOVA, vessels ≤ 15 μm, $P < 0.05$). While both tissues show a fractalkine-induced constriction, the difference in vessel kinetic response likely reflects the different systems used to explore microglial vasoregulation (ex vivo and in vivo, respectively).

Since the *Cx3cr1*$^{GFP/GFP}$ retina showed no fractalkine-induced vessel constriction, microglial contact with retinal vessels and neurons was explored. High-resolution immunocytochemical analysis of microglia (Fig. 2*D*, EGFP, green) contact with neuronal synapses (Fig. 2*D*, VGLUT1, red) and vessels (Fig. 2*D*, IB4, light blue) allowed specific areas of contact to be quantified. When the volume of contact per individual microglia was calculated, *Cx3cr1*$^{GFP/GFP}$ animals had fewer vessel contacts than animals with one functional copy of Cx3cr1 (Fig. 2*E*) (*Cx3cr1*$^{GFP/+}$ 7.5 ± 0.4% vs. *Cx3cr1*$^{GFP/GFP}$ 5.5 ± 0.3%, *t* test $P = 0.004$). While there was no difference in neuronal contacts between the two genotypes, *Cx3cr1*$^{GFP/GFP}$ animals showed less microglial process branching (Fig. 2*E*) (*Cx3cr1*$^{GFP/+}$ 111.5 ± 7.2 vs. *Cx3cr1*$^{GFP/GFP}$ 92.2 ± 2.1, *t* test $P = 0.03$), reflecting the literature showing *Cx3cr1*$^{GFP/GFP}$ to have a more activated inflammatory profile (29). When retinal capillary diameters were compared to C57bl6 control animals, *Cx3cr1*$^{GFP/+}$ capillaries were similar to controls (Fig. 2*F*) (C57bl6 11.3 ± 0.3 μm vs. *Cx3cr1*$^{GFP/+}$ 10.9 ± 0.2 μm, one-way ANOVA $P = 0.66$), while *Cx3cr1*$^{GFP/GFP}$ showed increased capillary diameters (Fig. 2*F*) (*Cx3cr1*$^{GFP/+}$ 10.9 ± 0.2 μm vs. *Cx3cr1*$^{GFP/GFP}$ 12 ± 0.4 μm, one-way ANOVA $P = 0.047$). There was no difference in larger vessel diameter for any genotype (Fig. 2 *F*, *Inset*) ($P = 0.87$ and 0.94 for *Cx3cr1*$^{GFP/+}$ and *Cx3cr1*$^{GFP/GFP}$, respectively).

RNA sequencing (RNA-seq) was performed on FACS-isolated microglia collected from 12-wk-old dark agouti rats to determine whether microglia expressed vasomodulatory factors. To confirm the purity of sample, the mapped genes were compared to a published list of microglial markers (30), with 23 of 29 markers identified in our gene population, including the microglial-specific marker *Tmem119* (*SI Appendix*, Table S1) (31). The negative microglial fraction (CD11b$^-$) was also interrogated for microglial signature genes, with key genes, such as *Cx3cr1*, *TMEM119*, and *Slc2a5* hardly expressed (<3 copies in >1 × 10^7 transcripts) (*SI Appendix*, Table S1). The microglial transcriptome was also compared to microglial-enriched genes reported in several studies, with significant overlap observed, while there was little contamination from known neuronal genes (*SI Appendix*, Fig. S5). The gene population was compared against genes known to be involved in angiogenesis (gene ontology [GO]:0001525, 407 genes) and regulation of blood

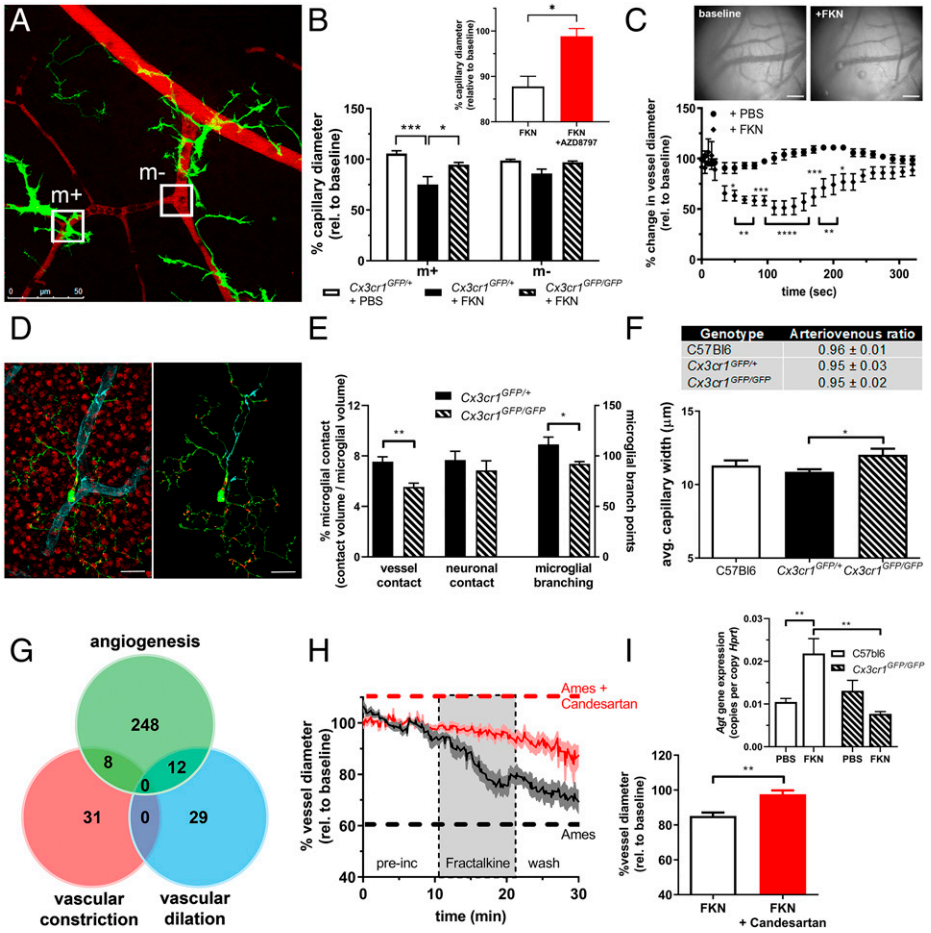

Fig. 2. Microglia constrict retinal capillaries via fractalkine-Cx3cr1 signaling and express genes for vasoactive agents. (*A*) Ex vivo *Cx3cr1*$^{GFP/+}$ retinae (EGFP; microglia, green) were labeled with Rhodamine B (blood vessels, red) and imaged under live cell microscopy. (Scale bar, 50 µm.) (*B*) The addition of fractalkine (200 ng/mL) induced vasoconstriction at sites of microglial contact (m+, $n = 4$ PBS, $n = 6$ FKN), while no significant vessel alteration occurred in areas lacking microglial processes (m−, $n = 5$ PBS, $n = 6$ FKN). When performed on *Cx3cr1*$^{GFP/GFP}$ retinae, no constriction was evident ($n = 5$). Supporting a Cx3cr1-mediated effect, the addition of the small-molecule Cx3cr1 inhibitor, AZD8797, blocked vasoconstriction (*Inset*, $n = 4$ FKN, $n = 3$ FKN+AZD8797). (*C*) The response of brain vasculature to fractalkine was tested in rat thin scull preparations, with constriction evident 120 s postinjection ($n = 3$ PBS, FKN). The *Insets* show representative images at baseline and after fractalkine addition. (Scale bar, 250 µm.) (*D*) Retinal microglia (EGFP, green), neuronal synapses (VGLUT1, red), and blood vessels (IB4, light blue) were imaged in *Cx3cr1*$^{GFP/+}$ and *Cx3cr1*$^{GFP/GFP}$ animals and the extent of vascular and neuronal contact quantified relative to microglial volume (see isolated microglia: red, neuronal contacts; blue, vascular contacts). (Scale bar, 15 µm.) (*E*) Grouped data showed *Cx3cr1*$^{GFP/GFP}$ retinae to have reduced vascular contacts compared to *Cx3cr1*$^{GFP/+}$ retinae ($n = 5$), while there was no difference in neuronal contacts. *Cx3cr1*$^{GFP/GFP}$ microglia exhibited reduced process branching ($n = 5$). (*F*) Using in vivo OCTA, retinal capillary diameter was increased in *Cx3cr1*$^{GFP/GFP}$ animals compared to *Cx3cr1*$^{GFP/+}$ retinae ($n = 4$ C57Bl6, $n = 6$ *Cx3cr1*$^{GFP/+}$, *Cx3cr1*$^{GFP/GFP}$), while there was no alteration in the diameter of arterioles or venules (A/V ratio shown in table, $n = 4$ C57Bl6, $n = 6$ *Cx3cr1*$^{GFP/+}$, $n = 5$ *Cx3cr1*$^{GFP/GFP}$). (*G*) RNA-seq was performed on FACS-isolated rat retinal microglia, with 268 genes identified as being angiogenic (GO:0001525), while 39 genes were involved in vascular constriction and 41 genes in vascular dilation (regulation of blood vessel diameter, GO:0097746). (*H*) Vessel diameter was quantified in rat retinal explants preincubated in Ames (black trace) or Ames + 230 nM candesartan (red trace) for 10 min, after which fractalkine (FKN, 200 ng/mL) was added (shaded area, representative data from 1 retina, $n = 5$ vessels). (*I*) When grouped data were analyzed 10 min after fractalkine addition, constriction was abolished when preincubated with candesartan ($n = 7$ fractalkine, $n = 5$ fractalkine + candesartan). Further supporting a role for the RAS, ex vivo incubation with fractalkine up-regulated microglial *Agt* expression, while this was not evident in microglia isolated from *Cx3cr1*$^{GFP/GFP}$ retinae (*Inset*, $n = 6$). Data expressed as mean ± SEM, $^*P < 0.05$, $^{**}P < 0.01$, $^{***}P < 0.001$, $^{****}P < 0.0001$.

vessel diameter (GO:0097746, 310 genes). In total, 268 genes expressed in the microglial population were identified to have roles in angiogenic pathways (Fig. 2*G* and *SI Appendix*, Table S2), such as hypoxia inducible factor 1α (*Hif1a*) and vascular endothelial growth factor A and B (*Vegf A*/*B*). When vessel diameter regulation was explored, 41 genes were found to have a role in vasodilation, such as phospholipase A2 (*Pla2g6*) and sirtuin 1 (*Sirt1*), while 39 genes were identified with vasoconstriction, including endothelin 1, -3 (*Edn1, -3*) and arachidonate 5-lipoxygenase (*Alox5*) and angiotensinogen (*Agt*) (Fig. 2*G*, and *SI Appendix*, Tables S3 and S4, respectively).

As angiotensinogen is a constituent of the renin-angiotensin system (RAS), which is involved in retinal vessel regulation via the angiotensin II receptor type 1 (AT1R) (32, 33), ex vivo experiments were performed using the AT1R antagonist, candesartan. Baseline capillary diameter was averaged over 10 min in rat retinal explants exposed to Ames (black trace) and Ames + candesartan (230 nM) (Fig. 2*H*, red trace) and after which time fractalkine was added (shaded area in Fig. 2*H*). Similar to that observed in the *Cx3cr1*$^{GFP/+}$ mouse (Fig. 2 *A* and *B*), exposure of the rat retinae to fractalkine induced capillary constriction, while candesartan blocked any fractalkine-induced constriction (Fig. 2*H*). When grouped data were analyzed, candesartan abolished the fractalkine-induced vasoconstriction (Fig. 2*I*) (80.4 ± 2.0% vs. 97.5 ± 2.3%, *t* test, $P < 0.01$).

To further support the role of RAS in microglial-mediated vessel regulation, control C57bl6 and *Cx3cr1*$^{GFP/GFP}$ were exposed ex vivo to fractalkine for 2 h, microglia isolated, and the expression of *Agt* quantified (Fig. 2*I*, *Inset*). While exposure to fractalkine increased *Agt* expression in control retinae, *Cx3cr1*$^{GFP/GFP}$ retinae that previously exhibited no microglial-mediated constriction (Fig. 2*B*) showed no expression change (Fig. 2*I*, *Inset*) (+FKN, C57bl6 21.8 ± 3.5 copies per 1,000 copies *Hprt* vs. *Cx3cr1*$^{GFP/+}$ 7.7 ± 0.6 copies per 1,000 copies *Hprt*, two-way ANOVA $P = 0.017$). The present data show that microglia are capable of modulating vascular constriction within the retina and broader regions of the CNS via the fractalkine-Cx3cr1 pathway. While microglia express several gene transcripts for known vasoactive agents, fractalkine-induced microglial regulation of retinal vessels occurs via AT1R.

Retinal Blood Flow and Capillary Diameter Is Changed in Early Diabetes. The regulation of retinal blood supply is critical to normal function, with retinal pathologies, such as DR, exhibiting early retinal blood flow defects and abnormal neurovascular

coupling (23, 25, 34). To explore whether microglial vasoregulation was altered during early diabetes, adult dark agouti rats were rendered diabetic via streptozotocin (STZ) with significant hyperglycemia evident throughout the 4-wk experimental period (*SI Appendix*, Table S5).

As reduced retinal blood flow is a consistent and early alteration in patients with diabetes and animal models (24, 25), quantitative vessel-dependent kinetic analysis using sodium fluorescein (35) was used to confirm vascular dysfunction. Average normalized fluorescence intensity was calculated over time for every pixel within the fundus image (Fig. 3 *A–C*, *Insets*), grouped on vessel type, and *en face* heat-maps produced (Fig. 3 *A–C*, fill times), with warmer colors indicating greater time taken to fill (slower blood flow). Vessel-dependent kinetic analysis revealed arterioles in STZ-treated animals took longer to fill (Fig. 3*D*) (median regression analysis, $P < 0.05$), reflecting reduced blood flow. Due to the serial nature of the retinal vasculature, this increase in fill time was also observed in retinal capillaries and venules (Fig. 3*D*) (median regression analysis, $P < 0.05$), with no vessel-specific deficit identified (median regression analysis, $P > 0.05$). Drain times were also longer in all retinal vessels (Fig. 3*E*) (median regression analysis, $P < 0.05$), with the effect significantly greater than that observed for fill times (median regression analysis, $P < 0.05$). The reduced arteriolar and venular blood flow in STZ-treated animals was verified using velocimetry (*SI Appendix*, Fig. S6) and the clinically relevant arterio-venous transit time was also exhibited reduced blood flow (increased transit time) (*SI Appendix*, Fig. S6*D*). The decrease in retinal blood flow was independent of systemic change, with systolic blood pressure, blood hematocrit, and intraocular pressure unaltered (*SI Appendix*, Fig. S7).

As vessel change affects blood flow in DR (36, 37), the morphology of large-diameter vessels was assessed from fluorescein images at peak fluorescent intensity. No change in large vessel tortuosity (Fig. 3*F*) (two-way ANOVA, arterioles $P = 0.52$, venules $P = 0.98$), or arteriole/venule diameter (arteriovenous ratio) (Fig. 3 *F*, *Inset*) (*t* test, $P = 0.48$) was observed between the two cohorts. Similarly, when arteriole, capillary and venule densities were separately quantified using retinal whole-mount immunohistochemistry (Fig. 3 *G*, *Inset* shows the rendered image of arterioles, dark blue; venules, cyan; and capillaries, yellow), no change in vessel densities were observed between control and STZ-treated animals (Fig. 3*G*) (two-way ANOVA, arterioles $P = 0.98$, venules $P = 0.99$, capillaries $P = 0.94$). As fluorescein image analysis and immunohistochemistry lack the resolution to assess capillary diameter, optical coherence tomography angiography (OCTA) was used to quantify this in vivo. Images of the superficial retinal capillary network were obtained for control (Fig. 3*H*) and STZ-treated (Fig. 3 *H*, *Inset*) animals and quantification (Fig. 3*H*, green overlay showing measured capillaries) revealed decreased capillary diameter in the STZ-treated cohort (Fig. 3*I*) (two-way ANOVA, $P < 0.05$). When a similar analysis was performed on the intermediate and deep capillary plexi, no change was detected (Fig. 3*I*) (two-way ANOVA, $P = 0.72$).

In summary, retinal blood flow was significantly slower in diabetes, with in vivo OCTA revealing retinal capillary constriction within the superficial vascular plexus 4 wk after STZ-induced diabetes. These diameter changes were restricted to the capillary network, as larger vessels remained unaltered and there was no change in retinal vascular coverage.

Retinal Microglia Contact with Capillaries and Pericytes Is Increased in Early Diabetes, Independent of Activation. The extent of microglial (Fig. 4 *A*, *Inset*, green, Iba-1) contact with arterioles, capillaries, and venules (Fig. 4 *A*, *Inset*, red, IB4) was quantified for control and STZ-treated animals to determine whether the retinal capillary constriction in diabetes was accompanied by altered microglial association. While microglia exhibited a similar association with large-diameter arterioles and venules (Fig. 4*A*) (two-way ANOVA, $P > 0.99$ and $P > 0.66$, respectively), microglial–capillary association was increased in STZ-treated animals (Fig. 4*A*) (two-way ANOVA, $P < 0.05$). In addition, microglial–pericyte association (Fig. 4 *B*, *Inset*, microglia green, Iba-1; pericytes light blue, NG2, vessels red, IB4) was increased within the central retina of STZ-treated animals (Fig. 4*B*) (two-way ANOVA, $P < 0.05$). There was no vessel dropout (Fig. 3*G*), nor loss of retinal pericytes (*SI Appendix*, Fig. S8) at this early stage of diabetes.

The association of microglia with pericytes and capillary areas lacking pericyte contact was further explored in control and STZ-treated animals using quantitative image analysis (Fig. 4 *C*, *Inset,* rendered image showing pericyte somata red; pericyte processes green; pericyte-free vessel blue and skeletonised microglia). While there was no specific preference for microglia to contact pericyte somata, processes or capillary areas lacking pericytes (Fig. 4*C*) (two-way ANOVA, $P = 0.16$), there was increased microglial association with all three at 4 wk of diabetes (Fig. 4*C*) (two-way ANOVA, $P < 0.01$). To determine whether this microglial effect was specific, or a result of a more generalized macroglial response as has been shown in later stages of diabetes (38, 39), astrocyte density and Müller cell gliosis were quantified. Vessel-specific astrocyte coverage (Fig. 4*D*) and Müller cell gliosis (Fig. 4*E*) were unaltered after 4-wk STZ treatment (two-way ANOVA, $P > 0.92$ and 0.99, respectively).

Previous work has shown blood-retinal barrier (BRB) integrity is compromised early in diabetes (40). Using vessel-dependent blood flow analysis (Fig. 3 *A–E*), we used the return to baseline after fluorescein peak (fluorescein offset) as a measure of BRB integrity. While no alteration in offset was observed for larger vessels, retinal capillaries showed a significant increase, indicative of fluorescein leakage/reduced BRB integrity (Fig. 4*F*) (median regression analysis, $P < 0.05$). A breakdown in BRB can lead to immune cell infiltration and microglia activation, with microglial migration and morphological change indicative of classic activation observed 1 mo post-STZ (41). To assess whether altered microglial–vessel association occurred in the context of monocyte involvement/microglial activation, whole-mounts were colabeled with IB4 and Iba-1 and the number and morphology of microglia quantified in central and peripheral retina. Despite the increase in capillary fluorescein offset, there was no difference in the number of monocytes/retinal microglia (Fig. 4*G*) (two-way ANOVA, central $P = 0.4$, peripheral $P = 0.9$), or microglial morphology after 4 wk of hyperglycemia (Fig. 4*H*) (two-way ANOVA, cell body area $P > 0.99$, process length/cell $P = 0.15$, branch points/cell $P > 0.99$). Despite this, *Cx3cr1* and fractalkine expression was increased in the diabetic retina (*SI Appendix*, Fig. S9). RNA-seq analysis of microglial isolates from 4-wk control and STZ-treated animals showed that of the 254 differentially expressed genes, 22 inflammatory response genes were identified, 15 of which were positive regulators (GO:0050729), while 12 were negative regulators of inflammation (GO:0050728) (Fig. 4*I* and *SI Appendix*, Tables S6 and S7). Importantly, chemokine and cytokines normally associated with microglial activation—including Tlr2, Il-1β, Cxcl10, TNF-a, IL-1a, C1q—were not altered and there was no expression of the infiltrating monocyte marker gene, *Ccr2*, in our RNA-seq dataset (31, 42). Thus, at this early stage of diabetes (4 wk) when retinal capillaries are constricted, there is increased microglial–capillary interaction, which is independent of monocyte recruitment, classic microglial activation, and a more generalized macroglial response.

Microglial Expression of Vasoactive Genes and Control of Capillary Constriction Are Altered in Early Diabetes. To determine whether there was a loss of retinal vasomotor control during early

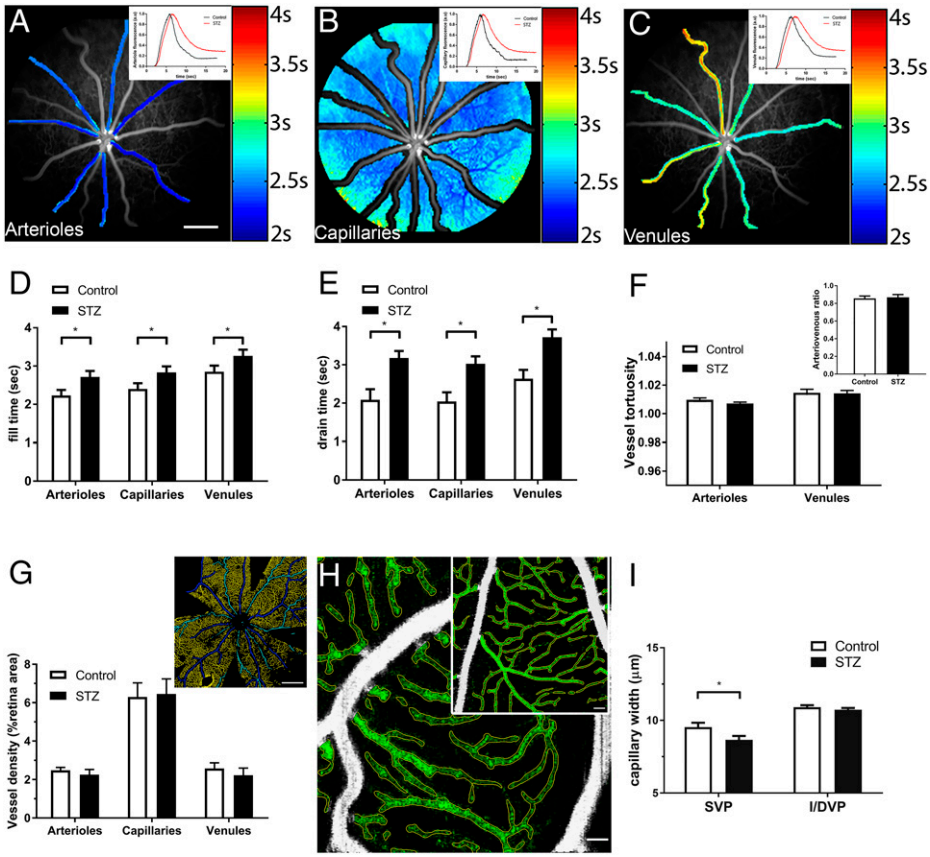

Fig. 3. Retinal blood flow is reduced and capillaries are constricted after 4 wk of diabetes. VFA was used to quantify retinal blood flow in control and STZ-treated animals. (*A*–*C*) *En face* heat-maps depicting fill time for arterioles, capillaries, and venules, with *Insets* showing representative average normalized fluorescence intensity traces for control (black line) and STZ-treated (red line) animals. (Scale bar, 500 μm in *A*.) (*D* and *E*) The times taken to reach half-maximum intensity (*D*, fill time) and half of final value from maximum (*E*, drain time) were quantified, showing fill and drain times were significantly increased in all vessel types in STZ-treated animals (unfilled bars, control $n = 23$; filled bars STZ, $n = 21$). (*F*) Sodium fluorescein fundus images were quantified for large vessel tortuosity ($n = 13$) and arteriovenous ratio (*Inset*, $n = 13$), with no difference observed between STZ-treated (filled bars) and control (unfilled bars) animals. (*G*) Immunohistochemistry was used to quantify vascular density in control and STZ-treated (unfilled and filled bars) eyes, with no difference observed between the two groups ($n = 11$). The rendered image shows the segmented vessel types (*Inset*, capillaries in yellow, arterioles in blue, and venules in cyan). (Scale bars, 1 mm.) (*H*) OCTA was performed in vivo to measure capillary diameter in control and STZ-treated (*Inset*) animals, with the vessels measured shown in green. (Scale bar, 50 μm.) (*I*) Decreased capillary diameter was observed in STZ-treated animals ($n = 12$) compared to control ($n = 10$) within the superior vascular plexus. No alteration was observed in the intermediate/deep vascular plexi. Group data expressed as mean ± SEM, $^*P < 0.05$.

diabetes, breathable oxygen was used to induce hyperoxic challenge and capillary diameter within the superficial vascular plexus was quantified using OCTA (Fig. 5 *A*, *Upper*). While control animals showed a distinct vasoconstriction in response to 100% oxygen, no constriction was observed in STZ-treated animals (Fig. 5*A*) (two-way ANOVA, $P < 0.05$). To explore whether this dysfunction was also evident in microglial-mediated vessel constriction, ex vivo retinal explants from control and STZ-treated animals were exposed to fractalkine and capillary diameter quantified. While constriction was evident in the control cohort, this response was absent in the STZ-treated animals (Fig. 5*B*) (two-way ANOVA, control $P < 0.05$, STZ-treated $P = 0.99$). When microglia were isolated from 4-wk STZ-treated and control retinae and RNA-seq performed, angiotensinogen (*Agt*) expression was increased 2.4-fold (false-discovery rate [FDR] = 0.009), while expression of the aryl hydrocarbon receptor gene (*Ahr*), a negative regulator of the RAS (43), was also increased (3.6-fold, FDR = 0.002) (Fig. 5*C*). Importantly, neither of these genes (FDR = 0.91 for *Agt* and *Ahr*) nor any other transcript (FDR > 0.12) were changed in the CD-11b$^-$ population.

Based on the loss of vasomotor control in the diabetic retina and the dysregulation of the microglial RAS pathway, animals were rendered diabetic and treated with candesartan cilexetil or vehicle in their drinking water. At 4 wk post-STZ, capillary diameter and retinal blood flow were quantified. OCTA analysis of superficial retinal capillaries showed a decrease in diameter within the vehicle control group, similar to that observed in Fig. 3*I* (Fig. 5*D*) (91.8 ± 2%, two-way ANOVA, $P < 0.05$). This capillary constriction was not evident in STZ-treated animals exposed to candesartan, with diameters returning to control levels (Fig. 5*D*) (99.9 ± 1.8%, two-way ANOVA, $P > 0.99$). However, despite this, retinal blood flow remained slower, with arterio-venous transit time increased in the vehicle and candesartan STZ-treated animals (Fig. 5*E*) (median regression analysis $P < 0.05$ and $P < 0.001$, respectively). Quantification of larger retinal vessels (arterioles and venules) showed systemic delivery of candesartan resulted in an increase arteriovenous ratio in the STZ-treated animals compared to candesartan-treated control (Fig. 5*F*) (STZ 0.94 ± 0.01, control 0.84 ± 0.01, two-way ANOVA $P < 0.05$) and vehicle-treated control and STZ animals (Fig. 5*F*) (control 0.798 ± 0.03, STZ 0.86 ± 0.02, 2-way ANOVA $P < 0.001$ and 0.05, respectively).

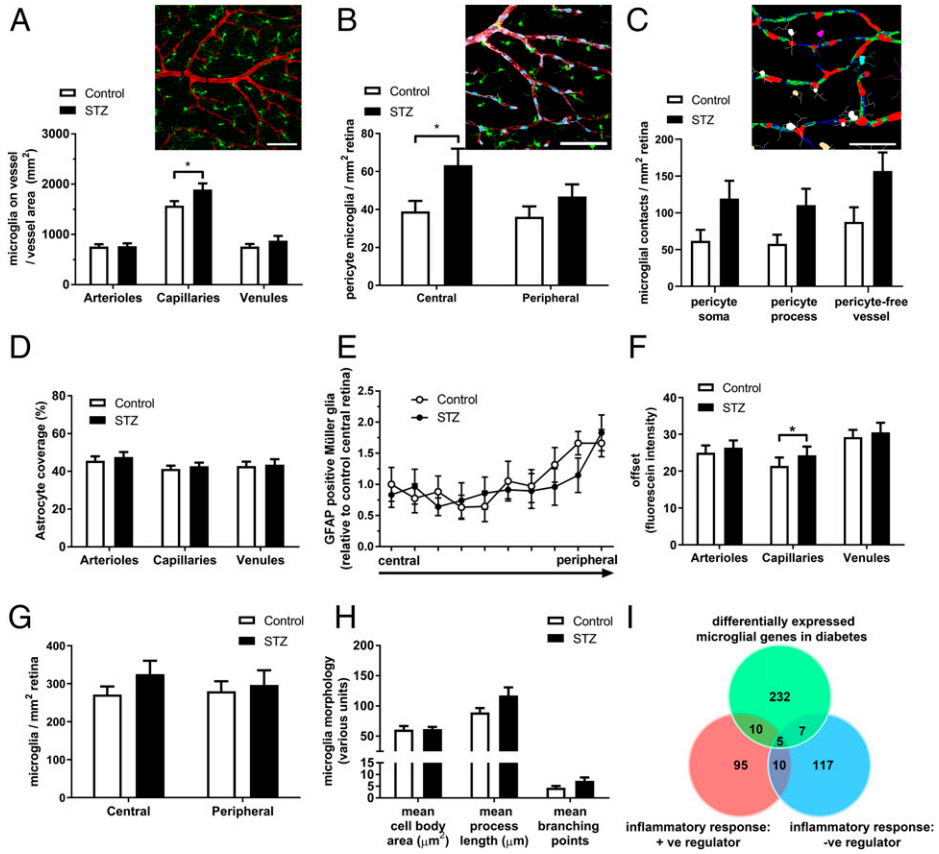

Fig. 4. Microglia increase their contact with retinal capillaries after 4 wk of STZ-induced diabetes. (*A*) Whole-mounted retina from control (*Inset*) and STZ-treated animals were labeled for Iba-1 (microglia, green) and IB4-FITC (blood vessels, red) and the extent of microglial and vessel contact quantified for each vessel type. While no difference in large vessel contacts occurred, microglia–capillary contact increased in the central retina of the STZ-treated animals (filled bars, $n = 11$). (Scale bar, 50 μm.) (*B*) Control (*Inset*) and STZ-treated animals were labeled for Iba-1 (microglia, green), NG2 (pericytes, light blue), and IB4-FITC (blood vessels, red) and the extent of microglia–pericyte contact quantified for each vessel type. Microglial–pericyte association increased within the central retina of STZ-treated animals (filled bars, $n = 11$). (Scale bar, 50 μm.) (*C*) Using similar immunolabeling as in *B,* microglial association with pericyte somata, processes, and capillary areas lacking pericyte contact was quantified. The image analysis render (*Inset*) highlights pericyte somata (red), pericyte processes (green), and pericyte-free vessels (blue), while microglia touching each of these regions were skeletonized and color-coded for quantification. While there were no preferential association, all contacts were increased in STZ-treated (filled bars, $n = 5$) compared to control (unfilled bars, $n = 5$) retinae (STZ treatment $P = 0.0015$). (Scale bar, 50 μm.) (*D* and *E*) Macroglial change was assessed in control (unfilled bars, $n = 11$) and STZ-treated (filled bars, $n = 11$) retinae, with no alteration in astrocyte coverage (*D*), nor Müller cell gliosis (*E*) observed ($n = 6$). (*F*) VFA was used to quantify fluorescein offset as a measure of BRB integrity. While arterioles and venules showed no change, capillary offset was increased in STZ-treated animals (unfilled bars, control $n = 23$; filled bars STZ, $n = 21$). (*G* and *H*) The inflammatory status of microglia was assessed morphologically and no difference was found in the number of monocytes/microglia in central and peripheral retina (*G*, $n = 11$), cell soma size, mean process length, or process branching points (*H,* $n = 5$ control, $n = 8$ STZ). (*I*) RNA-seq data from retinal microglia taken from control and STZ-treated rats were screened for genes involved in the positive (GO:0050729) and negative (GO:0050728) regulation of inflammation. While some inflammatory genes were altered, key inflammatory genes were unchanged after 4 wk of diabetes. Data represented as mean ± SEM, $^*P < 0.05$.

Overall, these data show that in early diabetes, retinal vasomodulation is aberrant, with a loss of microglial-mediated vasoconstriction and specific dysregulation of the RAS. However, treatment with the AT1R inhibitor, candesartan, did not restore retinal blood flow, despite dilating the retinal capillaries.

Discussion

The present study examined the role of microglia in local control of inner retinal blood supply. Microglia preferentially contact retinal capillaries that reside in the superficial vascular plexus, as well as contacting neuronal synapses within the inner retina. A role for microglia in vasomodulation within the retina and brain was identified, where addition of fractalkine induced capillary constriction. Subsequent characterization within the retina showed this vasomodulation to be dependent on microglial contact and Cx3cr1 signaling. The microglial transcriptome contained gene transcripts for known vasoactive agents, while the AT1R inhibitor, candesartan, blocked capillary constriction, suggesting microglial vasoregulation likely occurs via modulation of local RAS. This was supported by data showing fractakine-Cx3cr1–mediated up-regulation of angiotensinogen. Microglial vasoregulation was further explored in the context of vascular dysfunction during early diabetes. After 4 wk of experimental diabetes, retinal blood flow was reduced, coincident with constriction of retinal capillaries within the superficial plexus and increased microglial–capillary association. However, there was no indication of classic microglial activation, nor a more generalized macroglial response. RNA-seq data showed altered microglial expression of components of the RAS and there was a loss of microglial-mediated capillary constriction during diabetes. Finally, treatment with candesartan restored retinal capillary diameter in STZ-treated animals; however, retinal blood flow remained reduced.

Microglial Vasomodulation within the Retina. The present data show that microglia are intimately associated with retinal

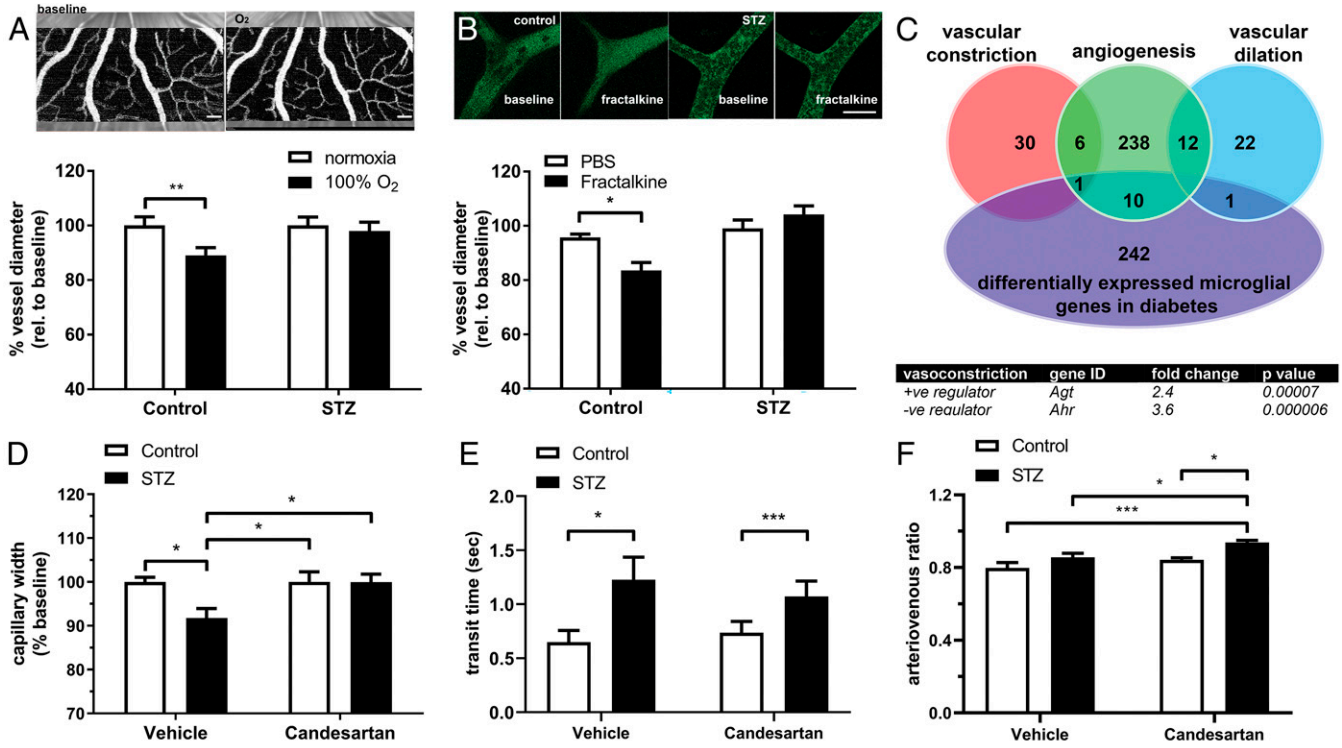

Fig. 5. Vasoactive gene expression from retinal microglia and fractalkine-induced vasoconstriction are altered after 4 wk of STZ-induced diabetes. (*A*) The responsiveness of retinal vessels to hyperoxic challenge was explored in vivo using OCTA (*Insets* show OCTA images from baseline and after exposure to O_2). (Scale bar, 200 μm.) While hyperoxic challenge (filled bars) lead to constriction in the control group (n = 10 normoxia, n = 6 100% O_2), no constriction was observed in the STZ cohort (n = 12 normoxia, n = 7 100% O_2). (*B*) Microglial vasoregulation was investigated during diabetes, with 4-wk STZ-treated and control retinae exposed to fractalkine ex vivo (representative control and STZ images in *Inset*) (Scale bar, 50 μm.) While vessels from control retinae showed fractalkine-induced vasoconstriction (filled bar), STZ retinae exhibited no change (n = 5 animals). (*C*) Differential microglial gene expression data from 4 wk control and STZ-treated animals were compared to vasomodulatory gene lists (vasoconstriction, GO:0097746; angiogenesis, GO:0001525; vasodilation, GO:0097746), with the RAS positive regulator angiotensinogen (*Agt*), and negative regulator (*Ahr*) significantly altered (FDR-adjusted, citrate control n = 5, STZ n = 4). (*D*) OCTA was used to quantify retinal superficial capillary diameter in 4-wk control and STZ-treated animals (unfilled and filled bars, respectively) exposed to candesartan or vehicle. In STZ-treated animals, capillary diameter returned to baseline in the candesartan-treated group (n = 7 control, n = 8, 5 STZ vehicle and candesartan, respectively). (*E*) Retinal blood flow was quantified using arterio-venous transit time and showed increased transit time (slower blood flow) in STZ-treated animals independent of candesartan treatment (n = 8 control, n = 11 and 8 STZ vehicle and candesartan, respectively). (*F*) Quantification of the arteriovenous ratio showed candesartan treatment increased the diameter of larger vessels in STZ-treated retinae relative to control and vehicle-treated tissues (n = 8 control, n = 11 and 8 STZ vehicle and candesartan, respectively). Data expressed as mean ± SEM, $*P < 0.05$, $**P < 0.01$, $***P < 0.001$.

vasculature, directly apposing pericytes and capillary areas free from pericytes, yet showing no particular preference for direct contact. Highlighting the functional significance of this interaction, stimulation of the microglial-specific receptor Cx3cr1 via its sole ligand fractalkine induced vasoconstriction, not only within the mouse and rat retina, but also in the brain. While the role of fractalkine-induced vessel constriction in the brain requires significantly more work to confirm microglial/Cx3cr1 involvement in areas exhibiting constriction, within the retina this effect was spatially discrete, occurring only in areas associated with microglial processes and was dependent on Cx3cr1 signaling, with $Cx3cr1^{GFP/GFP}$ retinae exhibiting no constriction, altered microglia-vessel contact and capillary diameter. While the previously reported alterations in the retina of $Cx3cr1^{GFP/GFP}$ mice may impact on these vascular outcomes (44), the Cx3cr1 inhibitor AZD8797 data showing a lack of fractalkine-induced constriction, is in agreement with the $Cx3cr1^{GFP/GFP}$ results, directly implicating microglia in the capillary response to fractalkine. While previous work has identified microglia as a component of the blood–brain barrier (45), and involved in retinal and brain vascular development (20, 46), this report of microglial-mediated vasomodulation is unique. Furthermore, our data and those of others show microglia also monitor and modulate neuronal synapses during development, throughout adulthood, and in response to activity (17, 47, 48), raising the possibility that microglia may contribute to neurovascular coupling, the process through which local blood flow is regulated by neuronal activity. As previous work in the retina suggests the existence of Müller cell-independent vasoregulatory mechanisms (11, 12), microglial vasoregulation may constitute one such alternative pathway, particularly within the superficial plexus. Further work exploring the structure of microglial–neuronal contact, its temporal response to altered neuronal activity, and its fractalkine dose–response profile will be required to properly characterize the role of microglia in the neurovascular unit.

Microglial RAS Involvement in Capillary Constriction. In order for microglia to directly mediate vessel constriction, they must express vasoactive factors. The RNA-seq data from isolated retinal microglia highlighted several genes for vasoactive agents, including endothelin (*Edn1, 3*), angiotensinogen (*Agt*), and arachidonate 5-lipoxygenase (*Alox5*), all of which are known to regulate retinal capillary tone (49). While retinal neuronal/glial cell contamination may confound the genes identified within the microglial isolate, the low levels of neuronal signature genes

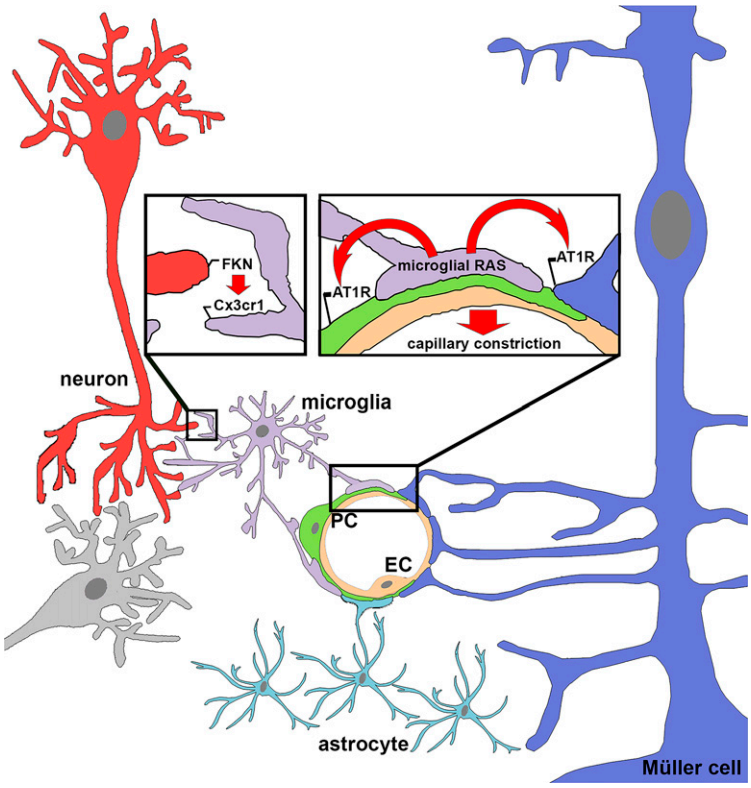

Fig. 6. Schematic representation of microglial regulation of retinal capillary constriction. Data from this study show microglia are structurally and functionally capable of involvement in the neurovascular unit. Microglia contact neuronal synapses and retinal capillaries (including pericytes) and activation of fractalkine-Cx3cr1 signaling results in capillary constriction, which is via an AT1R-dependent mechanism. Ultimately, capillary regulation may occur via direct microglial mechanism or may involve contributions from pericytes and Müller cells. EC, endothelial cell; PC, pericyte.

(*SI Appendix*, Fig. S5) suggest any effect would be minor. Importantly, preincubation with the AT1R antagonist, candesartan, inhibited microglial-mediated vasoconstriction and incubation with fractalkine induced up-regulation of microglial *Agt* expression, which was not observed when Cx3cr1 was genetically ablated. These data, together with the dysregulated microglial genes identified during diabetes (*Agt* and *Ahr*), implicate the RAS in microglial-mediated vasoregulation. All components of the RAS have been observed within the retina, with angiotensin II (AngII) implicated in the vasoconstriction of all retinal vessels (arterioles, capillaries, and venules) via AT1R (32, 33). While this microglial-mediated vasoregulation via the RAS is novel, microglia are known to express components of this pathway, including angiotensin-converting enzyme, AT1R, AT2R (50). In addition to vessel constriction via microglial RAS, microglial activation and inflammatory cytokine production has been described after AngII exposure within the brain and retina (51, 52). Thus, the modulation of microglial RAS in normal tissue may be required for normal vessel control, while during pathology there may be a positive feedback cycle involving AngII, promoting microglial activation and inflammation.

Given the ultrastructural and immunocytochemical data suggesting microglia contact pericyte somata and processes, it is possible that microglia communicate directly with pericytes and utilize their vasomodulatory capacity (5) in order to constrict inner retinal capillaries. Supporting communication between both cell types, pericytes are able to modulate microglial phenotype during inflammation (53), while AT1R are expressed by pericytes enabling AngII-mediated constriction (33). Furthermore, in vitro evidence suggests pericytes express fractalkine, while both fractalkine and Cx3cr1 gene transcripts have been identified in the pericyte transcriptome (54, 55). In addition to pericytes, our data also show that microglia could elicit a response by communicating directly with endothelial cells (capillary areas free of pericytes), which are also known to express vasoregulatory substances (56). Finally, microglia may indirectly communicate with vessels via other retinal glia, such as Müller cells, which express components of the RAS (57) and have been previously shown to regulate the inner retinal vasculature (9, 10). While a proposed mechanism is shown in Fig. 6, more work is required to explain how microglia signal to other members of the neurovascular unit to induce capillary constriction.

Microglial Involvement in Capillary Constriction during Early Diabetes and Its Effect on Retinal Blood Flow. Our finding of reduced retinal blood flow throughout all retinal vessel types in response to short duration hyperglycemia is supported by studies in both humans with diabetes and animal models of the disease (25). In contrast to larger retinal vessels that showed no alteration, there was a significant reduction in capillary diameter ($\sim -9\%$) within the superficial plexus. To our knowledge this is a unique finding and while the change in capillary diameter is small, it would lead to large effect on blood flow, since capillaries constitute the majority of retinal vasculature (58). One estimate indicated a 6% dilation in capillary diameter (~0.32 μm) generated the majority of blood flow increase evoked by neuronal activity (5). In addition to static vessel change, retinal capillaries from STZ-treated animals failed to constrict after hyperoxic challenge. This report of in vivo retinal capillary diameter measurement during vascular challenge is unique; however, previous human studies have reported altered hyperoxic retinal vessel responses (blood flow) in patients with type 1 (59) and type 2 (60) diabetes.

As changes in capillary network have been suggested to underlie the pathophysiology of early and later-stage DR (25, 61, 62), it is tempting to speculate that microglial control of these vessels contribute to the vascular dysfunction in early diabetes. The data showing an increase in the number of microglial processes associated with capillaries, increased microglial *Agt* expression, and the restoration of capillary diameter after candesartan cilexetil treatment all support this hypothesis. Even the increased microglial expression of aryl hydrocarbon receptor (*Ahr*), a negative regulator of vasoconstriction (43), may be incorporated into this theory,

since recent work shows it contributes to vessel stiffness (63). Therefore, the increased *Ahr* and *Agt* expression may contribute to the phenotype of smaller and less-responsive retinal blood vessels in early diabetes. Additional support for a microglial-specific effect on the retinal vasculature during diabetes comes from work in STZ-treated $Cx3cr1^{GFP/GFP}$ animals, which showed increased acellular capillaries after 4 mo of hyperglycemia (64). Further work using the STZ-treated $Cx3cr1^{GFP/GFP}$ model is required to specifically explore the capillary constriction evidenced early in diabetes.

The microglial dysregulation of the RAS suggests this pathway is altered in diabetes. These data are supported by our supplementary data (*SI Appendix*, Fig. S9) and previous studies showing increased angiotensinogen within the vitreous of individuals with proliferative DR (65) and increased vitreal AngII concentrations and elevated retinal AngII, AT1R, and AT2R levels in rodent models of diabetes (66, 67). As well as causing vasoconstriction, AngII is also known to uncouple pericytes from the endothelium, thereby altering vessel permeability and contributing to the development of microaneurysms, a key clinical determinant of DR (33). Validating the positive effects of candesartan on capillary vessel diameter and providing further support for the role of the RAS in DR, an earlier clinical trial showed candesartan blockade to be successful in preventing the onset of clinical grade DR in individuals with diabetes without DR (68). As these beneficial effects did not extend to preventing progression of DR in those with the disease, it suggests dysregulation of the RAS is relevant to the early, preclinical stage of DR.

Therefore, when the present data are considered together with the RAS dysregulation increased retinal fractalkine expression during diabetes [*SI Appendix*, Fig. S9 and other studies (69, 70)], a hypothesis can be formulated whereby in early diabetes, increased fractalkine expression together with enhanced microglial process-capillary interaction and altered microglial RAS, result in increased capillary vasoconstriction. While this potential role of microglial vasoregulation in DR is unique and unlike its inflammatory roles later in disease (41), further work is required to fully understand this early dysfunction and how it contributes to later pathology, such as the diminished hyperemic response observed in patients with diabetes (71, 72) and retinal hypoxia leading to later-stage DR (38, 73).

While candesartan blockade restored retinal capillary diameter to control levels in the present study, retinal blood flow remained decreased. This was surprising, as reversing capillary constriction would be expected to increase retinal blood flow, given the importance of the microvasculature (5, 58) and previous work showed candesartan cilexetil to restore blood flow in diabetic rats, albeit after 2 wk post-STZ (74). However, quantification of arteriovenous ratio in the candesartan-treated STZ animals showed increased diameter of these larger vessels. These data, in conjunction with previous work that showed AngII-dependent constriction of arterioles and venules (75), suggest that the dilation of the larger retinal vessels in the candesartan-treated STZ animals may result in reduced retinal blood velocity, masking the effect of dilated capillaries. A more targeted microglial RAS blockade may overcome these confounds and provide a clearer picture with respect to capillary dilation and retinal blood flow.

In summary, this study identifies a role for microglia in the modulation of capillaries within the CNS, particularly the retina. It highlights the involvement of the fractalkine-Cx3cr1 signaling axis and implicates the RAS in microglial-mediated capillary vasoregulation in the normal tissue and during the early stages of DR. While inhibition of the RAS pathway alters capillary constriction, it does not alter overall retinal blood flow in early diabetes. Further work investigating the cellular mechanism of microglial-induced vasoconstriction and intercellular signaling between microglia and other components of the neurovascular unit will provide valuable information on the retinal vascular response in health and disease.

Materials and Methods

Animals. Animal procedures were approved by the University of Melbourne Ethics Committee (#1613867) and adhered to the National Health and Medical Research Council of Australia guidelines and the *Guide for the Care and Use of Laboratory Animals* (76). To explore the role of microglia in retinal vasomodulation, $Cx3cr1^{GFP/+}$ and $Cx3cr1^{GFP/GFP}$ mice were used which have one or both alleles of the monocyte-specific receptor, *Cx3cr1*, replaced with EGFP (77). To show that Cx3cr1 labels microglia within healthy retina and not infiltrating monocytes, immunohistochemistry was performed with select markers (*SI Appendix*, Fig. S1). NG2-DsRed pericyte reporter mice were used to explore pericyte-microglial contact and were provided by B.T.S. Hyperglycemia was induced in male adult (6- to 8-wk-old) dark agouti rats via a single intraperitoneal injection of STZ (55 mg/kg, in trisodium citrate buffer, pH 4.5; Sigma-Aldrich), with control animals receiving an equivalent volume of vehicle. A separate cohort of animals was treated with candesartan cilexetil (10 μg/mL; Sigma-Aldrich, #SML0245) or vehicle (PEG400/Ethanol/Kolliphor EL/water, 10:5:2:83; Sigma-Aldrich) in their drinking water, 24 h after diabetes induction. In vivo imaging and tissue isolation was performed after 4 wk of diabetes.

Live Cell Imaging. Anesthetized $Cx3cr1^{GFP/+}$ and $Cx3cr1^{GFP/GFP}$ animals ($n = 5$ and 6, respectively) were injected intraperitoneally with rhodamine B (Sigma-Aldrich) to label blood vessels, since IB4 labeling on live cell explants showed microglia cross-reactivity (*SI Appendix*, Fig. S4). After 5 min, animals were overdosed (pentabarbitone phosphate, 120 mg/kg) and retinae dissected in chilled Ames medium (Sigma-Aldrich) prebubbled with carbogen (95% O_2, 5% CO_2). Retinae were imaged on an inverted confocal microscope (Leica SP5), perfused with 37 °C carbogenated Ames at 1 mL/min. Recombinant rat fractalkine (200 ng/mL; R&D Systems, #537-FT-025/CF) or vehicle (PBS) was introduced after 10 min of baseline recording and imaged for an additional 10 min. At the end of this incubation, vessel diameter was measured at sites with and without microglial contact (2 to 4 individual capillary sites per retina, $n = 4$ to 6 retinae) and measurements expressed as a percentage of baseline diameter of the same vessel region (taken as the average vessel diameter over the initial 10-min baseline). For quantification, the vessel imaging channel was separated from the microglia imaging channel and the scorer was blinded to microglial contact and treatment (PBS vs. FKN). In separate experiments, retinae were preincubated with the Cx3cr1 inhibitor, AZD8797 (10 μM; MedChemExpress, #HY-13848) or vehicle for 10 min prior to the addition of fractalkine (200 ng/mL). Ex vivo preparations were imaged for a total of 30 min to limit vessel caliber variability. While this ex vivo preparation may have limitations with respect to retinal blood flow, all explants were treated identically and all effects were relative to initial baseline. The vascular response to fractalkine after 4 wk of STZ-induced diabetes was measured using the above protocol, while to assess the role of the RAS in fractalkine-induced constriction, ex vivo retinae were preincubated in Ames or Ames + 230 nM candesartan cilexetil (Sigma-Aldrich) for 10 min. Fractalkine (200 ng/mL) was subsequently added and imaged for 10 min ($n = 5$ fractalkine + candesartan; $n = 7$ fractalkine), at which time vessel diameter was quantified relative to preincubation baseline. While candesartan cilexetil is a prodrug that is generally activated during gastrointestinal absorption, carboxyl esterases are present within the retina (78) and our previous work shows candesartan cilexetil blocks angiotensin-induced vessel effects when delivered directly to the eye (52).

In Vivo Video Fluorescein Angiography. For blood flow kinetic analysis of diabetic animals, in vivo video fluorescein angiography (VFA) was performed ($n = 21$ per group) as described previously using the Micron III rodent imaging system (Phoenix Research Labs) (35). This technique provides reliable quantification of blood flow kinetics using sodium fluorescein (1%, 100 μL/kg, fluorescite 10%; Alcon Laboratories). Additional details are provided in *SI Appendix*. The time taken from fluorescein entry into the retina to half-maximum intensity (fill time), and the time taken to fall from maximum intensity to the midpoint between maximum and final intensity after 30 s of imaging (drain time) were recorded.

In Vivo OCTA. To assess capillary diameter and capillary hyperoxic response in vivo, OCTA was performed (OCT2 Spectralis, Heidelberg Engineering). OCTA uses motion contrast imaging to generate real-time angiographic maps of the retinal vasculature (79). Volume scans (15 × 15° region of interest) were taken two to three disk diameters from the optic nerve. Each region consisted of 512 B-scans with each B-scan consisting of 512 A-scans. Superior and inferior retina were scanned in both eyes. The vascular response to hyperoxic conditions was measured in 4-wk STZ-treated and control animals by exposing the

animal to 100% oxygen via a nose cone (3 L/min). After a baseline image was taken, follow-up mode was used to acquire a second capillary image in the same retinal location, after 2 min of oxygen breathing.

Immunocytochemistry. Rat, mouse, and human retinae were processed for indirect immunofluorescence in whole-mount or cross-section, as previously described (80, 81). Retinal microglia were labeled with rabbit anti-ionized calcium-binding adapter molecule 1 (Iba-1, 1:1,000; Wako) or expressed EGFP (*Cx3cr1*$^{GFP/+}$, *Cx3cr1*$^{GFP/GFP}$), while blood vessels were visualized with *Griffonia simplicifolia* IB4 (FITC 1:75; Sigma-Aldrich; 647 fluorophore 1:100; Thermo Fisher Scientific). While IB4 has shown cross-reactivity with brain microglia and activated retinal microglia (82, 83), we observe no cross-reactivity in fixed retinal tissues. We also show better vessel coverage using IB4 compared to the endothelial marker CD-31 (*SI Appendix*, Fig. S10). Further details for immunolabeling are in *SI Appendix*. All imaging was performed at 20× on either Zeiss META/LSM800 confocals (Carl Zeiss) or Leica SP5 (Wetzlar), while high-resolution imaging of microglial-pericyte contact and EGFP expressing microglia was performed at 63×. For subsequent analysis of retinal whole-mounts, tile scans were taken at the superficial vascular plexus with *z*-stacks (15.6 μm) used to accommodate the variations in retinal mounting. All subsequent image analysis was performed on maximum-intensity projections.

Image Analysis.

Vessel morphology. Fundus images (n = 13 per group) were analyzed for arteriole/venule width and tortuosity in MATLAB (Mathworks) using the open-source plugin ARIA (84) at an eccentricity of 1.5 and 2 disk diameters from the optic nerve. Capillary width (<15 μm) within the superficial vascular plexus (OCTA) was measured using AngioTool (85). Confocal whole-mount images (n = 11 animals per group) were grouped into arterioles, venules, and capillaries based on their corresponding VFA profile and vessel masks used to segment subsequent analysis in Metamorph (Molecular Devices) using the angiogenesis tube-formation application. Total vessel area was quantified in NIH ImageJ (86) for each vessel type and vessel density was expressed as percentage of vessel area covering the total retinal area. For all subjective measurements, individuals were blinded to the treatment group.

Microglial, glial, pericyte histology, and vessel interaction. Microglia, pericytes, and astrocytes from STZ-treated and control tissue were analyzed in Metamorph utilizing the neurite outgrowth application. Iba-1$^+$ microglia were segmented, counted, and a mask generated. This microglial mask was overlaid on the vessel/pericyte masks and cells that overlapped with blood vessels by at least 0.82 μm were considered touching and were calculated as a percentage of total cells. For microglial blood vessel and neuronal contact in *Cx3cr1*$^{GFP/+}$ and *Cx3cr1*$^{GFP/GFP}$ retinae, areas of colocalization between individual microglia and vessels and synapses were rendered as a three-dimensional volume and expressed as a percentage of the total volume of the microglial cell (Imaris, Bitplane; three microglia per quadrant per retina, n = 5 animals per genotype). To further characterize microglial–pericyte interaction, a custom Metamorph script was used to quantify contacts (within 0.41 μm) between microglia (Iba-1$^+$) with pericyte somata and processes (NG2$^+$), as well as capillary areas devoid of pericyte contact (NG2$^-$, IB4$^+$, likely endothelial cells). Previous work has used EGFP in order to assess microglial contact with neurons in the retina and brain (17, 47, 87). Microglial morphology was also quantified using the automated neurite outgrowth application (Metamorph), while microglial–neuronal synapse and microglial–pericyte images were processed in Imaris. Astrocyte density within the ganglion cell layer was quantified for total retinal area and for overlap with each vessel type. Müller cell gliosis was quantified as previously described (44) (3 sections per animal, n = 6 animals).

Microglial Isolation and RNA-Seq. Retinae from control and 4-wk STZ-treated rats (n = 5 control, n = 4 STZ, 12-wk-old) were isolated, papain-digested (Worthington Biochemical), and labeled with CD11b-FITC conjugate (Miltenyi Biotec) for microglial isolation (FACSAria III, BD Bioscience). Both CD11b-FITC$^+$ (microglial-positive) and CD11b-FITC$^-$ (microglial-negative) fractions were collected. RNA was isolated and RNA-seq performed as in *SI Appendix*. To explore fractalkine regulation of microglial RAS, retinae from C57bl6 and *Cx3cr1*$^{GFP/GFP}$ animals (n = 6) were incubated as above with fractalkine (200 ng/mL; R&D Systems) or PBS for 2 h at 37 °C. Retinal microglia were isolated via FACS using the CD11b and EGFP labels. RNA was isolated and Smart-seq. 2 performed with 13 cycles of preamplification followed by quantitative PCR (*SI Appendix*).

Statistical Analysis. Statistical significance was determined by two-tailed unpaired Student's t test, two-way ANOVA, or repeated-measures ANOVA depending on the experiment (Prism 6.0, GraphPad). Where required, a Tukey post hoc analysis was performed. Blood flow analysis was undertaken using median regression analysis (STATA, StataCorp). Alpha levels were set at 0.05. Numerical values are expressed as SEM unless otherwise stated.

Data Availability. The data reported in this paper have been deposited in the Gene Expression Omnibus (GEO) database, https://www.ncbi.nlm.nih.gov/geo (accession no. GSE139276)(88).

ACKNOWLEDGMENTS. We thank Dr. Leonid Churilov for his assistance with statistical analysis; Dr. Christine Nguyen and Mr. Darren Zhao for their assistance with blood gas analysis; Ms. Satya Gunnam for her assistance with immunohistochemical staining and analysis; and the Biological Optical Microscopy and Melbourne Cytometry (MBC node) Platforms at the University of Melbourne. This work was supported by research grants from the National Health and Medical Research Council (APP-2000669, APP-1138509) and the Australian Research Council (DP160102642, DP200102001, FT130100338).

1. A. Ames III, Y. Y. Li, E. C. Heher, C. R. Kimble, Energy metabolism of rabbit retina as related to function: High cost of Na+ transport. *J. Neurosci.* **12**, 840–853 (1992).
2. D. Y. Yu, S. J. Cringle, Oxygen distribution and consumption within the retina in vascularised and avascular retinas and in animal models of retinal disease. *Prog. Retin. Eye Res.* **20**, 175–208 (2001).
3. J. P. Campbell *et al.*, Detailed vascular anatomy of the human retina by projection-resolved optical coherence tomography angiography. *Sci. Rep.* **7**, 42201 (2017).
4. T. E. Kornfield, E. A. Newman, Regulation of blood flow in the retinal trilaminar vascular network. *J. Neurosci.* **34**, 11504–11513 (2014).
5. C. N. Hall *et al.*, Capillary pericytes regulate cerebral blood flow in health and disease. *Nature* **508**, 55–60 (2014).
6. C. E. Riva, E. Logean, B. Falsini, Visually evoked hemodynamical response and assessment of neurovascular coupling in the optic nerve and retina. *Prog. Retin. Eye Res.* **24**, 183–215 (2005).
7. M. R. Metea, E. A. Newman, Signalling within the neurovascular unit in the mammalian retina. *Exp. Physiol.* **92**, 635–640 (2007).
8. T. Takano *et al.*, Astrocyte-mediated control of cerebral blood flow. *Nat. Neurosci.* **9**, 260–267 (2006).
9. E. A. Newman, Calcium increases in retinal glial cells evoked by light-induced neuronal activity. *J. Neurosci.* **25**, 5502–5510 (2005).
10. E. A. Newman, Functional hyperemia and mechanisms of neurovascular coupling in the retinal vasculature. *J. Cereb. Blood Flow Metab.* **33**, 1685–1695 (2013).
11. K. R. Biesecker *et al.*, Glial cell calcium signaling mediates capillary regulation of blood flow in the retina. *J. Neurosci.* **36**, 9435–9445 (2016).
12. A. Mishra, A. Hamid, E. A. Newman, Oxygen modulation of neurovascular coupling in the retina. *Proc. Natl. Acad. Sci. U.S.A.* **108**, 17827–17831 (2011).
13. J. A. Filosa, H. W. Morrison, J. A. Iddings, W. Du, K. J. Kim, Beyond neurovascular coupling, role of astrocytes in the regulation of vascular tone. *Neuroscience* **323**, 96–109 (2016).
14. J. G. Grigsby *et al.*, The role of microglia in diabetic retinopathy. *J. Ophthalmol.* **2014**, 705783 (2014).
15. J. Tang, T. S. Kern, Inflammation in diabetic retinopathy. *Prog. Retin. Eye Res.* **30**, 343–358 (2011).
16. U. K. Hanisch, H. Kettenmann, Microglia: Active sensor and versatile effector cells in the normal and pathologic brain. *Nat. Neurosci.* **10**, 1387–1394 (2007).
17. M. E. Tremblay, R. L. Lowery, A. K. Majewska, Microglial interactions with synapses are modulated by visual experience. *PLoS Biol.* **8**, e1000527 (2010).
18. M. E. Tremblay, A. K. Majewska, A role for microglia in synaptic plasticity? *Commun. Integr. Biol.* **4**, 220–222 (2011).
19. J. E. Lee, K. J. Liang, R. N. Fariss, W. T. Wong, Ex vivo dynamic imaging of retinal microglia using time-lapse confocal microscopy. *Invest. Ophthalmol. Vis. Sci.* **49**, 4169–4176 (2008).
20. D. Checchin, F. Sennlaub, E. Levavasseur, M. Leduc, S. Chemtob, Potential role of microglia in retinal blood vessel formation. *Invest. Ophthalmol. Vis. Sci.* **47**, 3595–3602 (2006).
21. B. Tan, E. Mason, B. MacLellan, K. K. Bizheva, Correlation of visually evoked functional and blood flow changes in the rat retina measured with a combined OCT+ERG system. *Invest. Ophthalmol. Vis. Sci.* **58**, 1673–1681 (2017).
22. N. Cheung, P. Mitchell, T. Y. Wong, Diabetic retinopathy. *Lancet* **376**, 124–136 (2010).
23. F. Tayyari *et al.*, Retinal blood flow and retinal blood oxygen saturation in mild to moderate diabetic retinopathy. *Invest. Ophthalmol. Vis. Sci.* **56**, 6796–6800 (2015).
24. S. E. Bursell *et al.*, Retinal blood flow changes in patients with insulin-dependent diabetes mellitus and no diabetic retinopathy. *Invest. Ophthalmol. Vis. Sci.* **37**, 886–897 (1996).
25. A. C. Clermont, S. E. Bursell, Retinal blood flow in diabetes. *Microcirculation* **14**, 49–61 (2007).
26. C. Y. Cheung, M. K. Ikram, R. Klein, T. Y. Wong, The clinical implications of recent studies on the structure and function of the retinal microvasculature in diabetes. *Diabetologia* **58**, 871–885 (2015).

27. N. Dudvarski Stankovic, M. Teodorczyk, R. Ploen, F. Zipp, M. H. H. Schmidt, Microglia-blood vessel interactions: A double-edged sword in brain pathologies. *Acta Neuropathol.* **131**, 347–363 (2016).
28. L. Cederblad, B. Rosengren, E. Ryberg, N. O. Hermansson, AZD8797 is an allosteric non-competitive modulator of the human CX3CR1 receptor. *Biochem. J.* **473**, 641–649 (2016).
29. S. Gyoneva *et al.*, *Cx3cr1*-deficient microglia exhibit a premature aging transcriptome. *Life Sci. Alliance* **2**, e201900453 (2019).
30. I. M. Chiu *et al.*, A neurodegeneration-specific gene-expression signature of acutely isolated microglia from an amyotrophic lateral sclerosis mouse model. *Cell Rep.* **4**, 385–401 (2013).
31. I. R. Holtman *et al.*, Induction of a common microglia gene expression signature by aging and neurodegenerative conditions: A co-expression meta-analysis. *Acta Neuropathol. Commun.* **3**, 31 (2015).
32. E. J. Rockwood, F. Fantes, E. B. Davis, D. R. Anderson, The response of retinal vasculature to angiotensin. *Invest. Ophthalmol. Vis. Sci.* **28**, 676–682 (1987).
33. H. Kawamura *et al.*, Effects of angiotensin II on the pericyte-containing microvasculature of the rat retina. *J. Physiol.* **561**, 671–683 (2004).
34. A. Mishra, E. A. Newman, Inhibition of inducible nitric oxide synthase reverses the loss of functional hyperemia in diabetic retinopathy. *Glia* **58**, 1996–2004 (2010).
35. F. Hui *et al.*, Quantitative spatial and temporal analysis of fluorescein angiography dynamics in the eye. *PLoS One* **9**, e111330 (2014).
36. J. W. Yau *et al.*, Meta-Analysis for Eye Disease (META-EYE) Study Group, Global prevalence and major risk factors of diabetic retinopathy. *Diabetes Care* **35**, 556–564 (2012).
37. R. Broe *et al.*, Retinal vessel calibers predict long-term microvascular complications in type 1 diabetes: The Danish Cohort of Pediatric Diabetes 1987 (DCPD1987). *Diabetes* **63**, 3906–3914 (2014).
38. A. Ly *et al.*, Early inner retinal astrocyte dysfunction during diabetes and development of hypoxia, retinal stress, and neuronal functional loss. *Invest. Ophthalmol. Vis. Sci.* **52**, 9316–9326 (2011).
39. E. Rungger-Brändle, A. A. Dosso, P. M. Leuenberger, Glial reactivity, an early feature of diabetic retinopathy. *Invest. Ophthalmol. Vis. Sci.* **41**, 1971–1980 (2000).
40. A. Carmo, J. G. Cunha-Vaz, A. P. Carvalho, M. C. Lopes, Effect of cyclosporin-A on the blood–retinal barrier permeability in streptozotocin-induced diabetes. *Mediators Inflamm.* **9**, 243–248 (2000).
41. X. X. Zeng, Y. K. Ng, E. A. Ling, Neuronal and microglial response in the retina of streptozotocin-induced diabetic rats. *Vis. Neurosci.* **17**, 463–471 (2000).
42. C. Feng *et al.*, Expression of CCL2 and its receptor in activation and migration of microglia and monocytes induced by photoreceptor apoptosis. *Mol. Vis.* **23**, 765–777 (2017).
43. A. K. Lund, M. B. Goens, N. L. Kanagy, M. K. Walker, Cardiac hypertrophy in aryl hydrocarbon receptor null mice is correlated with elevated angiotensin II, endothelin-1, and mean arterial blood pressure. *Toxicol. Appl. Pharmacol.* **193**, 177–187 (2003).
44. A. I. Jobling *et al.*, The role of the microglial Cx3cr1 pathway in the postnatal maturation of retinal photoreceptors. *J. Neurosci.* **38**, 4708–4723 (2018).
45. B. V. Zlokovic, The blood-brain barrier in health and chronic neurodegenerative disorders. *Neuron* **57**, 178–201 (2008).
46. T. Arnold, C. Betsholtz, Correction: The importance of microglia in the development of the vasculature in the central nervous system. *Vasc. Cell* **5**, 12 (2013).
47. D. P. Schafer *et al.*, Microglia sculpt postnatal neural circuits in an activity and complement-dependent manner. *Neuron* **74**, 691–705 (2012).
48. X. Wang *et al.*, Requirement for microglia for the maintenance of synaptic function and integrity in the mature retina. *J. Neurosci.* **36**, 2827–2842 (2016).
49. C. J. Pournaras, E. Rungger-Brändle, C. E. Riva, S. H. Hardarson, E. Stefansson, Regulation of retinal blood flow in health and disease. *Prog. Retin. Eye Res.* **27**, 284–330 (2008).
50. S. J. Liu *et al.*, Gastrodin attenuates microglia activation through renin-angiotensin system and Sirtuin3 pathway. *Neurochem. Int.* **120**, 49–63 (2018).
51. N. Torika, K. Asraf, E. Roasso, A. Danon, S. Fleisher-Berkovich, Angiotensin converting enzyme inhibitors ameliorate brain inflammation associated with microglial activation: Possible implications for Alzheimer's disease. *J. Neuroimmune Pharmacol.* **11**, 774–785 (2016).
52. J. A. Phipps *et al.*, The role of angiotensin II/AT1 receptor signaling in regulating retinal microglial activation. *Invest. Ophthalmol. Vis. Sci.* **59**, 487–498 (2018).
53. J. Matsumoto *et al.*, Tumor necrosis factor-α-stimulated brain pericytes possess a unique cytokine and chemokine release profile and enhance microglial activation. *Neurosci. Lett.* **578**, 133–138 (2014).
54. Y. Shigemoto-Mogami, K. Hoshikawa, K. Sato, Activated microglia disrupt the blood-brain barrier and induce chemokines and cytokines in a rat in vitro model. *Front. Cell. Neurosci.* **12**, 494 (2018).
55. S. Chasseigneaux *et al.*, Isolation and differential transcriptome of vascular smooth muscle cells and mid-capillary pericytes from the rat brain. *Sci. Rep.* **8**, 12272 (2018).
56. K. Hamilton, L. Dunning, W. R. Ferrell, J. C. Lockhart, A. MacKenzie, Endothelium-derived contraction in a model of rheumatoid arthritis is mediated via angiotensin II type 1 receptors. *Vascul. Pharmacol.* **100**, 51–57 (2018).
57. L. E. Downie *et al.*, Neuronal and glial cell expression of angiotensin II type 1 (AT1) and type 2 (AT2) receptors in the rat retina. *Neuroscience* **161**, 195–213 (2009).
58. P. Blinder *et al.*, The cortical angiome: An interconnected vascular network with non-columnar patterns of blood flow. *Nat. Neurosci.* **16**, 889–897 (2013).
59. A. Harris *et al.*, Hyperoxia improves contrast sensitivity in early diabetic retinopathy. *Br. J. Ophthalmol.* **80**, 209–213 (1996).
60. M. E. Lott *et al.*, Impaired coronary and retinal vasomotor function to hyperoxia in individuals with type 2 diabetes. *Microvasc. Res.* **101**, 1–7 (2015).
61. A. Y. Kim *et al.*, Quantifying microvascular density and morphology in diabetic retinopathy using spectral-domain optical coherence tomography angiography. *Invest. Ophthalmol. Vis. Sci.* **57**, OCT362–OCT370 (2016).
62. J. M. Simonett *et al.*, Early microvascular retinal changes in optical coherence tomography angiography in patients with type 1 diabetes mellitus. *Acta Ophthalmol.* **95**, e751–e755 (2017).
63. A. Eckers *et al.*, The aryl hydrocarbon receptor promotes aging phenotypes across species. *Sci. Rep.* **6**, 19618 (2016).
64. E. Beli *et al.*, CX3CR1 deficiency accelerates the development of retinopathy in a rodent model of type 1 diabetes. *J. Mol. Med. (Berl.)* **94**, 1255–1265 (2016).
65. B. B. Gao, X. Chen, N. Timothy, L. P. Aiello, E. P. Feener, Characterization of the vitreous proteome in diabetes without diabetic retinopathy and diabetes with proliferative diabetic retinopathy. *J. Proteome Res.* **7**, 2516–2525 (2008).
66. I. S. Byon *et al.*, Effect of angiotensin II type 1 receptor blocker and angiotensin converting enzyme inhibitor on the intraocular growth factors and their receptors in streptozotocin-induced diabetic rats. *Int. J. Ophthalmol.* **10**, 896–901 (2017).
67. J. H. Kim, J. H. Kim, Y. S. Yu, C. S. Cho, K. W. Kim, Blockade of angiotensin II attenuates VEGF-mediated blood-retinal barrier breakdown in diabetic retinopathy. *J. Cereb. Blood Flow Metab.* **29**, 621–628 (2009).
68. N. Chaturvedi *et al.*, DIRECT Programme Study Group, Effect of candesartan on prevention (DIRECT-Prevent 1) and progression (DIRECT-Protect 1) of retinopathy in type 1 diabetes: Randomised, placebo-controlled trials. *Lancet* **372**, 1394–1402 (2008).
69. P. T. Yeh, H. W. Huang, C. M. Yang, W. S. Yang, C. H. Yang, Astaxanthin inhibits expression of retinal oxidative stress and inflammatory mediators in streptozotocin-induced diabetic rats. *PLoS One* **11**, e0146438 (2016).
70. P. T. Yeh *et al.*, Effect of fenofibrate on the expression of inflammatory mediators in a diabetic rat model. *Curr. Eye Res.* **44**, 1121–1132 (2019).
71. M. E. Lott *et al.*, Impaired retinal vasodilator responses in prediabetes and type 2 diabetes. *Acta Ophthalmol.* **91**, e462–e469 (2013).
72. A. Mandecka *et al.*, Influence of flickering light on the retinal vessels in diabetic patients. *Diabetes Care* **30**, 3048–3052 (2007).
73. G. B. Arden, S. Sivaprasad, Hypoxia and oxidative stress in the causation of diabetic retinopathy. *Curr. Diabetes Rev.* **7**, 291–304 (2011).
74. N. Horio *et al.*, Angiotensin AT(1) receptor antagonism normalizes retinal blood flow and acetylcholine-induced vasodilatation in normotensive diabetic rats. *Diabetologia* **47**, 113–123 (2004).
75. P. S. Kulkarni, H. Hamid, M. Barati, D. Butulija, Angiotensin II-induced constrictions are masked by bovine retinal vessels. *Invest. Ophthalmol. Vis. Sci.* **40**, 721–728 (1999).
76. National Research Council, *Guide for the Care and Use of Laboratory Animals* (National Academies Press, Washington, DC, ed. 8, 2011).
77. S. Jung *et al.*, Analysis of fractalkine receptor CX(3)CR1 function by targeted deletion and green fluorescent protein reporter gene insertion. *Mol. Cell. Biol.* **20**, 4106–4114 (2000).
78. S. Duvvuri, S. Majumdar, A. K. Mitra, Role of metabolism in ocular drug delivery. *Curr. Drug Metab.* **5**, 507–515 (2004).
79. F. Y. Tang *et al.*, Determinants of quantitative optical coherence tomography angiography metrics in patients with diabetes. *Sci. Rep.* **7**, 2575 (2017).
80. K. A. Vessey *et al.*, Ccl2/Cx3cr1 knockout mice have inner retinal dysfunction but are not an accelerated model of AMD. *Invest. Ophthalmol. Vis. Sci.* **53**, 7833–7846 (2012).
81. A. I. Jobling *et al.*, Nanosecond laser therapy reverses pathologic and molecular changes in age-related macular degeneration without retinal damage. *FASEB J.* **29**, 696–710 (2015).
82. W. Ma *et al.*, Absence of TGFβ signaling in retinal microglia induces retinal degeneration and exacerbates choroidal neovascularization. *eLife* **8**, 8 (2019).
83. A. Lünemann *et al.*, Macrophage/microglia activation factor expression is restricted to lesion-associated microglial cells after brain trauma. *Glia* **53**, 412–419 (2006).
84. P. Bankhead, C. N. Scholfield, J. G. McGeown, T. M. Curtis, Fast retinal vessel detection and measurement using wavelets and edge location refinement. *PLoS One* **7**, e32435 (2012).
85. E. Zudaire, L. Gambardella, C. Kurcz, S. Vermeren, A computational tool for quantitative analysis of vascular networks. *PLoS One* **6**, e27385 (2011).
86. C. A. Schneider, W. S. Rasband, K. W. Eliceiri, NIH Image to ImageJ: 25 years of image analysis. *Nat. Methods* **9**, 671–675 (2012).
87. A. M. Fontainhas *et al.*, Microglial morphology and dynamic behavior is regulated by ionotropic glutamatergic and GABAergic neurotransmission. *PLoS One* **6**, e15973 (2011).
88. S. A. Mills *et al.*, RNAseq analysis of retinal microglia during early diabetes. Gene Expression Omnibus. https://www.ncbi.nlm.nih.gov/geo/query/acc.cgi?acc=GSE139276. Deposited 19 October 2019.